

Article

Mechanical and Tribological Behavior of Nitrided AISI/SAE 4340 Steel Coated with NiP and AlCrN

Marcos E. Soares ¹, Qianxi He ^{2,*}, Jose M. DePaiva ^{2,*}, Bruna M. de Freitas ³, Paulo Soares ³, Stephen C. Veldhuis ², Fred L. Amorim ³ and Ricardo D. Torres ³

¹ Mechanical Engineering Department, Universidade Tecnológica Federal do Paraná (UTFPR), Ponta Grossa 84017-220, Brazil

² McMaster Manufacturing Research Institute (MMRI), McMaster University, Hamilton, ON L8S 4L8, Canada

³ Mechanical Engineering Department, Pontifícia Universidade Católica do Paraná (PUCPR), Curitiba 80215-901, Brazil

* Correspondence: heq19@mcmaster.ca (Q.H.); paivajj@mcmaster.ca (J.M.D.)

Abstract: In this study, novel surface engineering strategies to improve the wear performance of AISI 4340 were investigated. The strategies were as follows: (i) NiP deposition on a previously nitrided steel substrate, followed by NiP interdiffusion heat treatment at either 400 °C or 610 °C (referred to as duplex treatment); (ii) the deposition of AlCrN PVD coating on NiP layers on a previously nitrided steel substrate (referred to as triplex treatment). Prior to the deposition of AlCrN, the NiP was subjected to the interdiffusion heat treatment at either 400 °C or 610 °C. These strategies were compared with the performance of the AlCrN coating directly applied on nitrided steel. To characterize the microstructural features of each layer, X-ray diffraction (XRD) and scanning electron microscopy (SEM) coupled with energy-dispersive X-ray spectroscopy (EDS) analysis were conducted. We also carried out mechanical and tribological behavior assessments. The tribological tests were carried out using a ball-on-disc tribometer under a constant load of 20 N and a tangential speed of 25 cm/s; cemented carbide spheres with a diameter of 6 mm were the counterpart body. The friction coefficient was continuously monitored throughout the tests. The results reveal that the wear mechanism for the AlCrN coating is predominantly oxidative. The most wear-resistant surface architecture was the one comprising AlCrN over the NiP layer subjected to interdiffusion heat treatment at either 400 °C or 610 °C.

Keywords: AlCrN/NiP tribological behavior; AlCrN/NiP mechanical properties; duplex treatment; triplex treatment; electroless nickel



Citation: Soares, M.E.; He, Q.; DePaiva, J.M.; de Freitas, B.M.; Soares, P.; Veldhuis, S.C.; Amorim, F.L.; Torres, R.D. Mechanical and Tribological Behavior of Nitrided AISI/SAE 4340 Steel Coated with NiP and AlCrN. *Lubricants* **2024**, *12*, 181. <https://doi.org/10.3390/lubricants12050181>

Received: 7 March 2024

Revised: 3 May 2024

Accepted: 14 May 2024

Published: 17 May 2024



Copyright: © 2024 by the authors. Licensee MDPI, Basel, Switzerland. This article is an open access article distributed under the terms and conditions of the Creative Commons Attribution (CC BY) license (<https://creativecommons.org/licenses/by/4.0/>).

1. Introduction

Offshore oil exploration in the pre-salt region of the Brazilian continental platform, which can reach depths of 2000 to 5000 m, requires equipment with exceptional mechanical and corrosion properties. To withstand the demanding conditions of pre-salt oil exploration, various strategies are employed, including the use of corrosion-resistant alloys (CRA) such as Inconel 625 and super-duplex stainless steel, as well as the application of protective coatings, for instance, the application of carbon steel clad with Inconel 625 [1,2].

Ni-based coatings, particularly those containing phosphorous, are widely used in oil exploration equipment. The NiP coating, obtained through an acid-aqueous solution containing nickel sulfate and sodium hypophosphite, grows on the metal surface via an autocatalytic reaction, resulting in a uniform thickness on the steel surface [3,4]. In the oil exploration industry, a minimum P content of around 8% and a Ni-P thickness exceeding 75 µm are required to provide effective cathodic protection to the steel surface. However, as-deposited coatings with a high P content exhibit an amorphous structure with low mechanical properties [3,5].

To improve the mechanical and tribological performance of the NiP coating, an inter-diffusion post-heat treatment (IPHT) is commonly employed. The IPHT creates a metallurgical bond between the NiP deposit and the steel substrate, leading to the crystallization of the amorphous structure and the precipitation of the Ni₃P phase, thereby enhancing the coating's properties [5–11]. However, when the IPHT is conducted at the recommended temperature of 610 °C for an extended period (up to 10 h), a softening of the low-alloy steel substrate occurs due to the tempering temperature being lower (around 370 °C) than the IPHT temperature [12]. Consequently, the steel substrate loses the ability to sustain the load, which could cause the failure of the NiP coating.

To address this issue, previous studies have proposed matching the IPHT and tempering temperature at 600 °C, along with a shorter duration of 2 to 4 h [13]. This approach has been shown to enable the NiP-coated AISI/SAE 4140 steel to meet the mechanical requirements of ASTM 320 L7, which specifies alloy steel and stainless-steel bolting for low-temperature service. Additionally, plasma nitriding of the quenched/tempered substrate before NiP deposition, followed by IPHT at 400 °C or 610 °C, has been investigated [12]. This approach has been shown to enable the NiP-coated AISI/SAE 4140 steel to meet the mechanical requirements of ASTM 320 L7, which specifies alloy steel and stainless-steel bolting for low-temperature service. The results demonstrated that nitriding effectively prevents substrate softening, regardless of the IPHT temperature, with the nitriding effect being more prominent at 400 °C.

In contrast, physical vapor deposition (PVD) coatings, such as those deposited by cathodic arc evaporation (CAE) [14–16], sputtering, balanced magnetron sputtering (BMS), unbalanced magnetron sputtering (UBMS), and high-power impulse magnetron sputtering (HiPIMS) [17,18], among others, are rarely used in highly corrosion-aggressive environments such as the conditions found in offshore oil exploration. Direct application of PVD coatings on carbon or low-alloy steels presents limitations, including a low thickness (often less than 5 µm) that increases the risk of a coating system failure and epitaxial growth, which allows corrosion media to permeate into the coating and reach the steel substrate [17,19]. Droplets, especially in CAE-deposited coatings, often result in a localized absence of the coating material, promoting severe corrosion when exposed to corrosive media [20,21]. However, certain PVD coatings, such as TiAlN, AlTiN, AlCrN, and TiSiN/AlCrN, exhibit high hardness (up to 35 GPa), offering excellent wear and fatigue resistance. These coatings demonstrate enhanced performance when deposited on a nitrided substrate [22–25].

This study aims to investigate the tribological behavior of an AlCrN PVD coating on the NiP deposit on plasma-nitrided AISI/SAE 4340 steel specimens (Triplex). AlCrN is a PVD coating known for its high hardness and favorable tribological properties. The mechanical and tribological performance of NiP coatings, subjected to two different IPHT temperatures (400 °C and 610 °C) in the duplex architecture, are initially explored. Subsequently, in the triplex architecture, the impact of IPHT on the ability of the NiP deposit to provide mechanical support for the AlCrN coating and enhance its wear resistance is investigated.

2. Experimental Procedures

This study aims to investigate the tribological performance of the AlCrN on the NiP coating system with 5 different layer architectures. The experimental setup involved the following steps:

- Preparation of specimens: Several 5 mm disc specimens were obtained by cutting a 25 mm diameter AISI/SAE 4340 bar. These specimens served as the base material for the coating system investigation.
- Heat treatment: The steel specimens underwent heat treatment processes, including quenching and tempering (Q/T). This treatment optimized the mechanical properties of the specimens to ensure consistent and reliable results.

- Plasma nitriding: After the Q/T process, the quenched and tempered samples were subjected to plasma nitriding.

Figure 1 illustrates the 5 different layer architectures investigated in this project. Each architecture represents a specific combination of coatings and heat treatments:

- Duplex architecture 1 (AlCrN on nitrided steel): In this architecture, an approximately 3-micrometer-thick AlCrN coating was directly deposited onto the nitrided steel specimens. This architecture aimed to evaluate the tribological performance of the AlCrN coating on a nitrided substrate.
- Duplex architecture 2 and 3 (NiP on nitrided steel): In the second and third architectures, a 30-micrometer-thick NiP coating was deposited onto the nitrided substrates. Subsequently, interdiffusion post-heat treatment (IPHT) was performed at 400 °C or 610 °C. These architectures aimed to assess the effect of the IPHT temperature on the mechanical and tribological properties of the NiP coating.
- Triplex architecture 4 and 5 (AlCrN on NiP on nitrided steel): In the fourth and fifth architectures, an AlCrN coating was deposited using the cathodic arc evaporation (CAE) technique onto the NiP-coated substrates, which had undergone IPHT at 400 °C or 610 °C. These architectures aimed to investigate the influence of the IPHT on the ability of the NiP deposit to provide mechanical support for the AlCrN coating and enhance its wear resistance.

2.1. Steel Heat Treatment and Nitriding

The AISI/SAE 4340 steel disc specimens were subjected to a controlled heat treatment. The specimens were heated to 870 °C and held at this temperature for 1 h, followed by quenching in oil. Subsequently, the quenched specimens underwent tempering at 370 °C for 2 h. The resulting average hardness was approximately 45 HRC. Following this, the samples were cleaned and prepared metallographically to obtain a polished surface.

After the heat treatment, the steel specimens were submitted to plasma nitriding. The nitriding process was conducted in an in-house chamber. The nitriding environment consisted of 75% N₂ and 25% H₂, working pressure of 2 Torr, at 470 °C for 6 h. The average hardness of the hardened layer was 8.6 GPa, with a thickness around 300 µm. The surface of the nitrided specimens was prepared using 1200-grit sandpaper.

2.2. Electroless Nickel Deposition Process and AlCrN Coating

The electroless nickel (NiP) deposition process was carried out by immersing the nitrided steel specimens in an aqueous solution, with the following composition: 34 g/L of nickel sulfate, 35 g/L of sodium hypophosphite, 35 g/L malic acid, 10 g/L acid succinic, 5% v/v of ammonia hydroxide, and 1 ppm of thiourea. The nitrided specimens were kept for 2 h in the solution, with the solution temperature maintained at 90 °C and the pH controlled within a range of 4.5 to 5.5. The surface-to-solution volume ratio for the specimens was 0.67 dm²/L. This process resulted in an average NiP layer thickness of 20 µm, with a phosphorous content exceeding 10%. Subsequently, the NiP-coated samples were prepared using 1200-grit sandpaper.

The PVD coating applied on both nitrided and NiP-coated specimens was an AlCrN system deposited by the CAE/PVD method, according to the Alcrona-PRO[®] process at the Oerlikon Balzers facility (SJ Pinhais, Brazil). The AlCrN coating contains approximately 26 wt.% nitrogen, 38 wt.% aluminum, and 38 wt.% chromium.

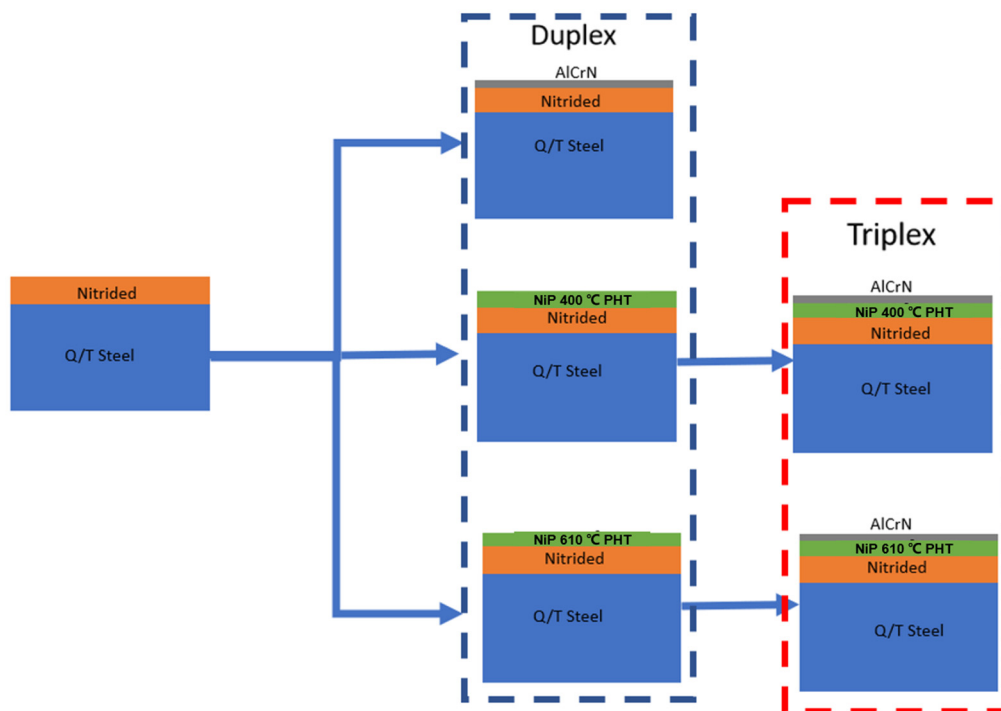


Figure 1. The duplex architectures: The AlCrN/nitrided steel, NiP IPHT at 400 °C/nitrided steel, NiP IPHT at 610 °C/nitrided steel. The triplex architectures: AlCrN/NiP IPHT at 400 °C/nitrided steel, AlCrN/NiP IPHT at 610 °C/nitrided steel architectures.

2.3. Characterization Techniques

2.3.1. Microstructural Characterization

The phase identification of the phases in the coating layers was obtained using X-ray diffraction (XRD) with a Shimadzu XRD-7000 instrument (Shimadzu—Kyoto, Japan), employing CuK α radiation ($\lambda = 1.54$ nm), with Grazing Incidence Angle geometry (GIXRD). We used a thin-film setting at either 1° or 2° incidence angle, scan speed of 0.5°/min and 0.02° step, with a 2 θ scan range from 20° to 80°. The diffracted peaks were indexed using the match function in the software and the ICDD PDF2+ database.

Microstructural analysis (morphology and thickness) of the coatings was carried out by inspecting the specimens' cross-section in a scanning electron microscope (Tescan—Vega3 SEM—Brno, Czech Republic).

2.3.2. Hardness and Elastic Modulus Determination

The determination of hardness (H) and reduced elastic modulus (E) was carried out by performing instrumented indentation tests normal to the outer layer of each architecture with a Berkovich tip, using a Dynamic Ultra Micro Hardness Tester Shimadzu DUH-211S (Shimadzu—Kyoto, Japan). During the indentation tests, a load of 50 mN was applied and held for 15 s at the maximum load. At least 10 indentations were made for each surface architecture. Hardness and reduced Young's modulus (E) values were extracted from load–displacement curves, using the Oliver and Pharr method.

2.3.3. Adhesion Tests

Adhesion was measured through scratch tests conducted on the surface of the coated specimens. These tests were performed under a scratch tester (Revestest, Anton-Paar, Corcelles, Switzerland), with a gradual application of force ranging from 1 N to 75 N with an HRC indenter, for a distance of 3 mm and at a speed of 6 mm/min. Subsequently, the failure modes were identified, and critical loads were assigned in accordance with the ASTM C 1624-5 standard [26].

2.3.4. Tribological Tests

The tribological tests were carried out using a ball-on-disc configuration in a universal tribometer (Revestest, Anton-Paar, Corcelles, Switzerland), according to the ASTM G99-17 Standard [27]. The tribological counterpart was a 6 mm cemented carbide ball. Sliding distances of 250, 500, and 1000 m, a speed of 25 cm/s, and a load of 20 N were employed for these tests. The coefficient of friction (CoF) was continuously recorded during the tests. Following the tests, the cross-sectional area of the wear track was measured using an optical profiler (Taylor-Robson CCI Lite—Leicester, England). The volume loss was determined by multiplying the cross-section area by the wear track's perimeter. Additionally, the wear mechanisms on the tracks were examined by SEM/EDS (Tescan, Vega3). The wear rate (WR) was calculated using the following equation:

$$WR = \frac{V}{F * L} \quad (1)$$

where V (mm^3) is the total volumetric wear, F (N) is the normal load, and L (m) is the sliding distance.

3. Results and Discussion

The Ra roughness values for all five surface architectures are presented in Table 1. The lowest roughness is for the duplex reference specimen, where the AlCrN coating was deposited onto a nitrided steel substrate. For polished plasma-nitrided steel surfaces, the roughness can be as low as 0.05 Ra. However, the CAE/PVD deposition process increases the roughness of the specimens due to the presence of droplets, which are large amounts of the deposited material that evaporate from the target and subsequently condense on the specimen's surface [20,21].

Table 1. Average roughness (Ra) for the 5 surface conditions.

Architecture of Coatings	Roughness, Ra (μm)
AlCrN-NiP400-Nitrided Steel	0.19 ± 0.01
AlCrN-NiP610-Nitrided Steel	0.21 ± 0.04
NiP400-Nitrided Steel	0.23 ± 0.07
NiP610-Nitrided Steel	0.31 ± 0.03
AlCrN-Nitrided Steel	0.15 ± 0.02

In cases where NiP was deposited on the nitrided surface, the roughness measured around 0.23 Ra and 0.31 Ra for the IPHT performed at 400 °C and 610 °C, respectively. The higher roughness of the NiP coatings is attributed to the surface topography that results from the NiP deposition process, which exhibits a cauliflower-like texture [28–30]. Furthermore, when the IPHT is performed at 610 °C, the Ni₃P coalesces, giving lower hardness than the NIP IPHT at 400 °C. Consequently, the IPHT specimens at 610 °C plastically deform, resulting in higher surface hardness, e.g., 0.31 Ra, than the specimens heat-treated at 400 °C, e.g., 0.23 Ra. However, when the AlCrN is deposited over the IPHT substrates at 400 °C or 610 °C, the surface roughness decreases and, practically, evens out.

The XRD patterns in Figure 2 depict the phases present in the five different architectural configurations. In the nitrided case, the ϵ -Fe_{2,3}N phases were observed. The NiP layer on the nitrided substrates exhibits similar phases, regardless of the post-heat treatment temperatures: Ni₃P and Ni phases. However, the NiO phase is only present in the NiP deposit subjected to IPHT at 610 °C. Notably, in Figure 3b, it can be observed that Ni₃P is an incoherent precipitate when the NiP deposit is IPHT at 610 °C. Conversely, the Ni₃P is not visible in Figure 3a, but its presence is confirmed by the XRD pattern in Figure 2, suggesting coherent precipitation.

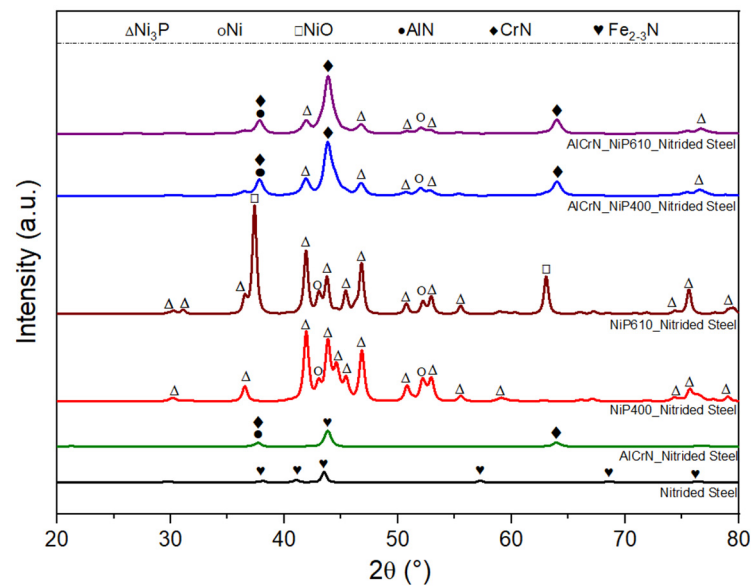


Figure 2. XRD of the nitrided steel plus XRD of the five architectures.

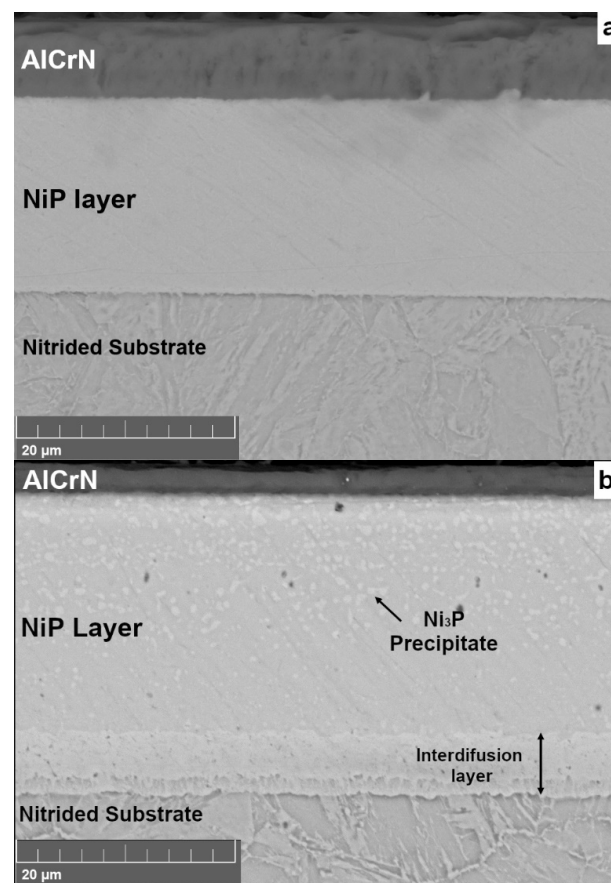


Figure 3. Cross-section of the (a) AICrN/NiP IPHT at 400 °C/nitrided steel and (b) AICrN/NiP IPHT at 610 °C/nitrided architectures.

The XRD pattern in Figure 2 shows AICrN peaks as AlN and CrN, both of which have an FCC crystal structure. Al and Cr interchange within this structure. The triplex architectures exhibit XRD diffraction patterns for both the AICrN and NiP layers. Figure 3a,b illustrate the cross-sections of the two triplex architectures. The thickness of AICrN is 5 μm and 3 μm for NiP IPHT at 400 °C and 610 °C, respectively. In contrast, the NiP thickness

is 18 μm and 20 μm for NiP IPHT at 400 $^{\circ}\text{C}$ and 610 $^{\circ}\text{C}$, respectively. Furthermore, the interdiffusion layer, formed during IPHT at 610 $^{\circ}\text{C}$, is approximately 5 μm thick and is not detectable in the coated system when the IPHT is performed at 400 $^{\circ}\text{C}$, as shown in Figure 3a.

Table 2 displays the hardness (H), reduced elastic modulus (E), and H/E ratio for the five architectures, along with the hardness of the nitrided case. In the nitrided case, the values for H and E are 6.62 and 262 GPa, respectively. These values align with recent findings for nitrided cases where the outer layer is $\epsilon\text{-Fe}_{2,3}\text{N}$, as indicated by the XRD diffraction pattern in Figure 2 [2,31]. The NiP IPHT at 610 $^{\circ}\text{C}$ shows H and E values of 11 and 206 GPa, respectively. The implementation of IPHT at this temperature results in four main effects: (i) the formation of an interdiffusion layer with a thickness of approximately 5 μm (Figure 3b); (ii) crystallization of the NiP coating; (iii) incoherent precipitation of Ni_3P (Figure 3b); (iv) formation of NiO due to the exposition of the coating to a rich air environment [6,32,33] (see XRD diffraction pattern in Figure 2). The first two effects contribute to an increase in the hardness of the NiP coating compared to the amorphous arrangements of P and Ni species. On the other hand, when the IPHT is conducted at 400 $^{\circ}\text{C}$, the interdiffusion layer has a submicron thickness. The Ni_3P precipitates coherently, resulting in higher mechanical properties, i.e., 14.67 and 227 GPa for H and E, respectively, compared to the NiP IPHT at 610 $^{\circ}\text{C}$ [32]. For the AlCrN on the nitrided steel substrate, the H and E values are 35.4 and 353 GPa, respectively. Typical H and E values for the AlCrN system range between 28 and 35 GPa and from 250 to 300 GPa, respectively, depending on the coating stoichiometry, deposition parameters, and other factors [19,34]. The H and E of the AlCrN coating on NiP IPHT at 400 $^{\circ}\text{C}$ are 34.88 and 348 GPa, respectively, while for AlCrN on the NiP IPHT at 610 $^{\circ}\text{C}$ are 30.79 and 338 GPa, respectively. The hardness and reduced elastic modulus are higher for the NiP IPHT at 400 $^{\circ}\text{C}$ due to the coherent precipitation of Ni_3P , consequently providing a higher load-bearing capacity for the AlCrN coating.

Table 2. Average values of H, E, and H/E ratio for the five architectures.

Layer Architecture	H (GPa)	E (GPa)	H/E
Nitrided Steel	6.62 \pm 0.31	262 \pm 5	0.025 \pm 0.0012
NiP 400/Nitrided Steel	14.67 \pm 1.26	227 \pm 9	0.064 \pm 0.003
NiP 610/Nitrided Steel	11.00 \pm 3.74	206 \pm 27	0.053 \pm 0.016
AlCrN/Nitrided Steel	35.50 \pm 4.80	353 \pm 38	0.100 \pm 0.013
AlCrN/NiP 400/Nitrided Steel	34.88 \pm 4.13	348 \pm 29	0.099 \pm 0.0038
AlCrN/NiP 610/Nitrided Steel	30.79 \pm 3.79	338 \pm 41	0.091 \pm 0.0074

Figure 4 illustrates the scratch grooves for the five different architectures, with Table 3 detailing the failure modes and corresponding critical loads of the scratch tests. Specifically, Figure 4a,b display the scratch groove characteristics for NiP interdiffusion post-heat treated (IPHT) at 400 $^{\circ}\text{C}$ and 610 $^{\circ}\text{C}$, respectively. Notably, both the NiP IPHT at 400 $^{\circ}\text{C}$ and 610 $^{\circ}\text{C}$ exhibit no delamination of the coating in the scratch grooves. This absence of delamination is attributed to two factors: (i) the NiP coating thickness is approximately 20 μm , and (ii) the NiP coating undergoes plastic deformation, rendering the standard adhesion principles applied to ceramic coatings on steel, such as nitrides, inapplicable to the NiP deposit. The scratch tests conducted in the NiP system evaluate the coating's ability to withstand stress generated by the HRC diamond stylus moving across the specimen surface. For instance, in the case of NiP IPHT at 400 $^{\circ}\text{C}$, stress accommodation at the test's onset results in the formation of arc tensile cracks ($\text{Lc1} = 3 \text{ N}$), occurring just after the HRC stylus has passed due to strain release. Subsequently, chevron tensile cracks form ($\text{Lc2} = 14 \text{ N}$), followed by wedging spallation ($\text{Lc3} = 33.5 \text{ N}$).

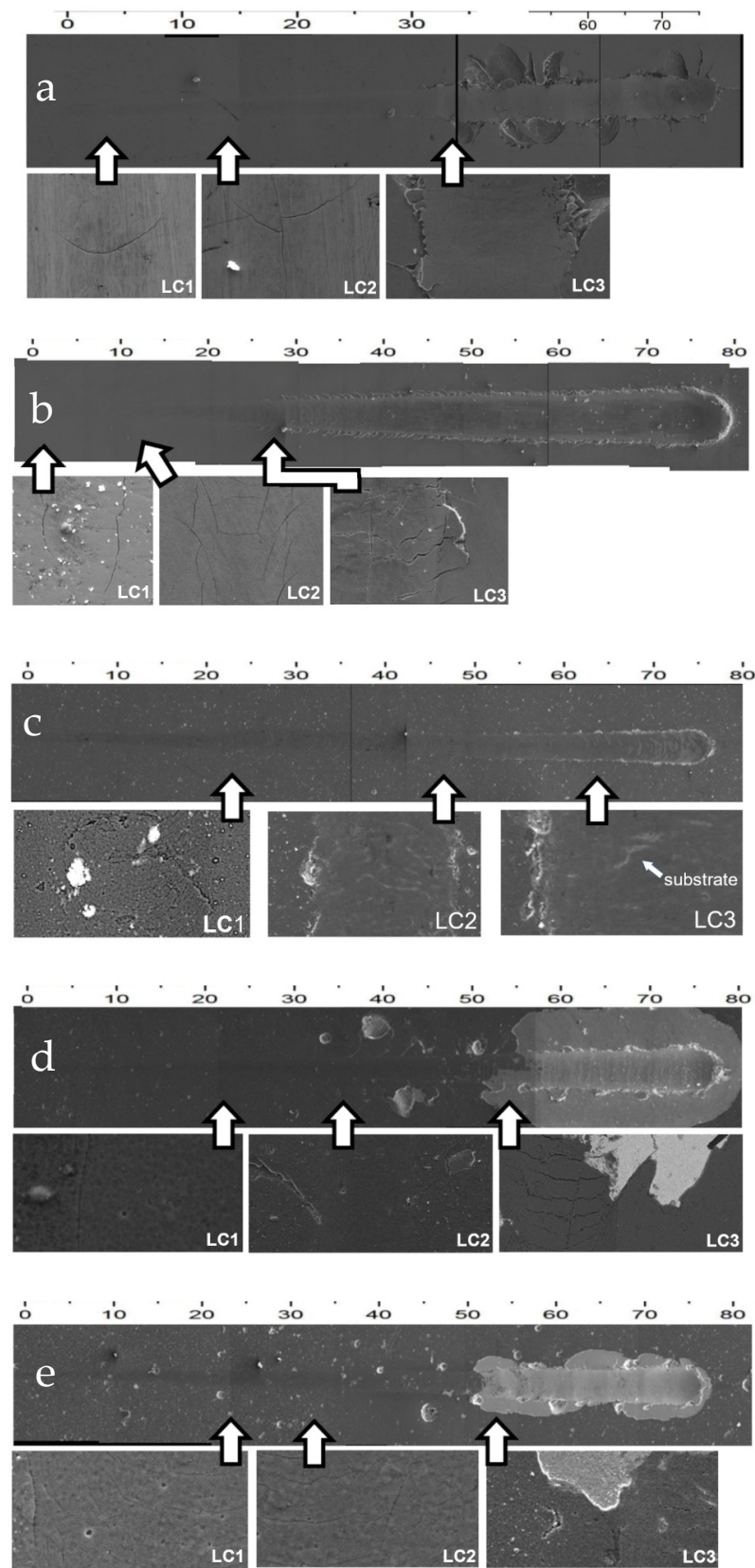


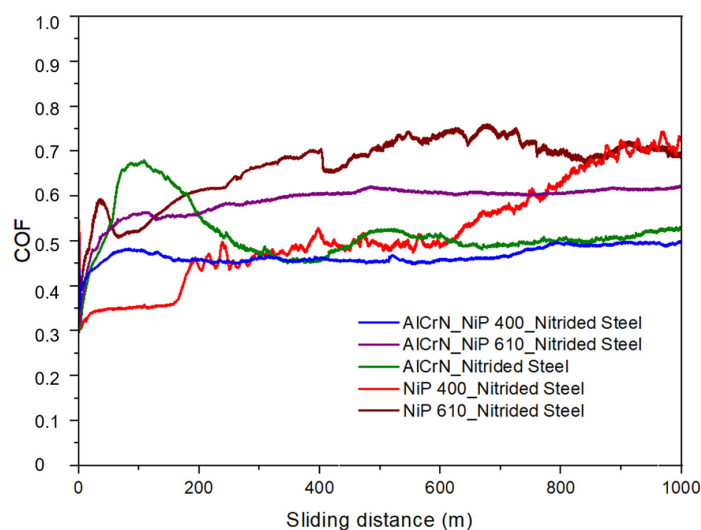
Figure 4. Aspect of the scratch groove: (a) NiP IPHT at 400 °C/nitrided Steel (b) NiP IPHT at 610 °C/nitrided steel, (c) AlCrN/nitrided steel (d) AlCrN/NiP IPHT at 400 °C/nitrided steel and (e) AlCrN/NiP IPHT at 610 °C/nitrided steel.

Table 3. Scratch test critical loads and failure modes of the five architectures.

Architecture	Lc1 (N)	Failure Mode	Lc2 (N)	Failure Mode	Lc3 (N)	Failure Mode
NiP IPHT 400 °C	3.0	arc tensile cracks	14.0	chevron tensile cracks	33.5	wedging spallation
NiP IPHT 610 °C	1.0	lateral cracks	10.0	chevron tensile cracks	28.0	wedging spallation
AlCrN/Nitrided Steel	22.5	conformal cracks	46.0	recovery spallation	63.0	buckling spallation
AlCrN/NiP 400 °C Nitrided Steel	22.0	lateral cracks	32.5	chevron tensile cracks	51.0	gross spallation
AlCrN/NiP 610 °C Nitrided Steel	25.0	lateral cracks	35.0	chevron tensile cracks	51.0	gross spallation

Conversely, NiP IPHT at 610 °C displays lateral cracks at the scratch groove's beginning (Lc1 = 1 N), succeeded by more substantial chevron tensile cracks (Lc2 = 10 N). This could be attributed to the interaction of the HRC stylus with the microstructure consisting of a Ni matrix with incoherent Ni₃P particles, providing an easy path for crack propagation. Finally, wedging spallation is also observed (Lc3 = 28 N). In Figure 4c, the scratch groove of AlCrN on the nitrided substrate reveals common failure modes for hard coatings over nitrided substrates. Conformal cracks emerge at 22.5 N (Lc1), followed by recovery spallation at 46 N (Lc2) and buckling spallation at 63 N (Lc3). The nitrided substrate enhances the adhesion of PVD coatings [35]. Finally, Figure 4d,e depict the scratch grooves for the two triplex architectures. These architectures exhibit failure modes, including lateral cracks, chevron tensile cracks, and gross spallation (Lc3) at a critical load of 51 N, indicating poor adhesion of AlCrN on the NiP layer, irrespective of the IPHT temperature. The root cause of this poor adhesion lies in the plastic deformation of the NiP deposit due to the presence of Ni in the microstructure, as depicted in Figure 2.

The coefficient of friction behavior, as a function of sliding distance for all architectures, is depicted in Figure 5. The friction coefficient behavior of the duplex structure and AlCrN on nitrided steel exhibits a notable increase, reaching its maximum between 100 and 130 m, indicative of the running-in stage associated with the removal of AlCrN droplets. This phenomenon is common in coatings deposited by cathodic arc evaporation (CAE/PVD). Subsequently, the coefficient of friction stabilizes at a steady-state condition of around 0.53, observed at a sliding distance of approximately 300 m. The primary wear mechanism is oxidative because chromium, aluminum, and oxygen signals overlap, according to energy-dispersive spectroscopy (EDS), not shown here, suggesting the formation of chromium–aluminum oxides (refer to Figure 6c). The wear rate (Figure 7) remains constant throughout the sliding distance.

**Figure 5.** Friction coefficient behavior of the five architectures.

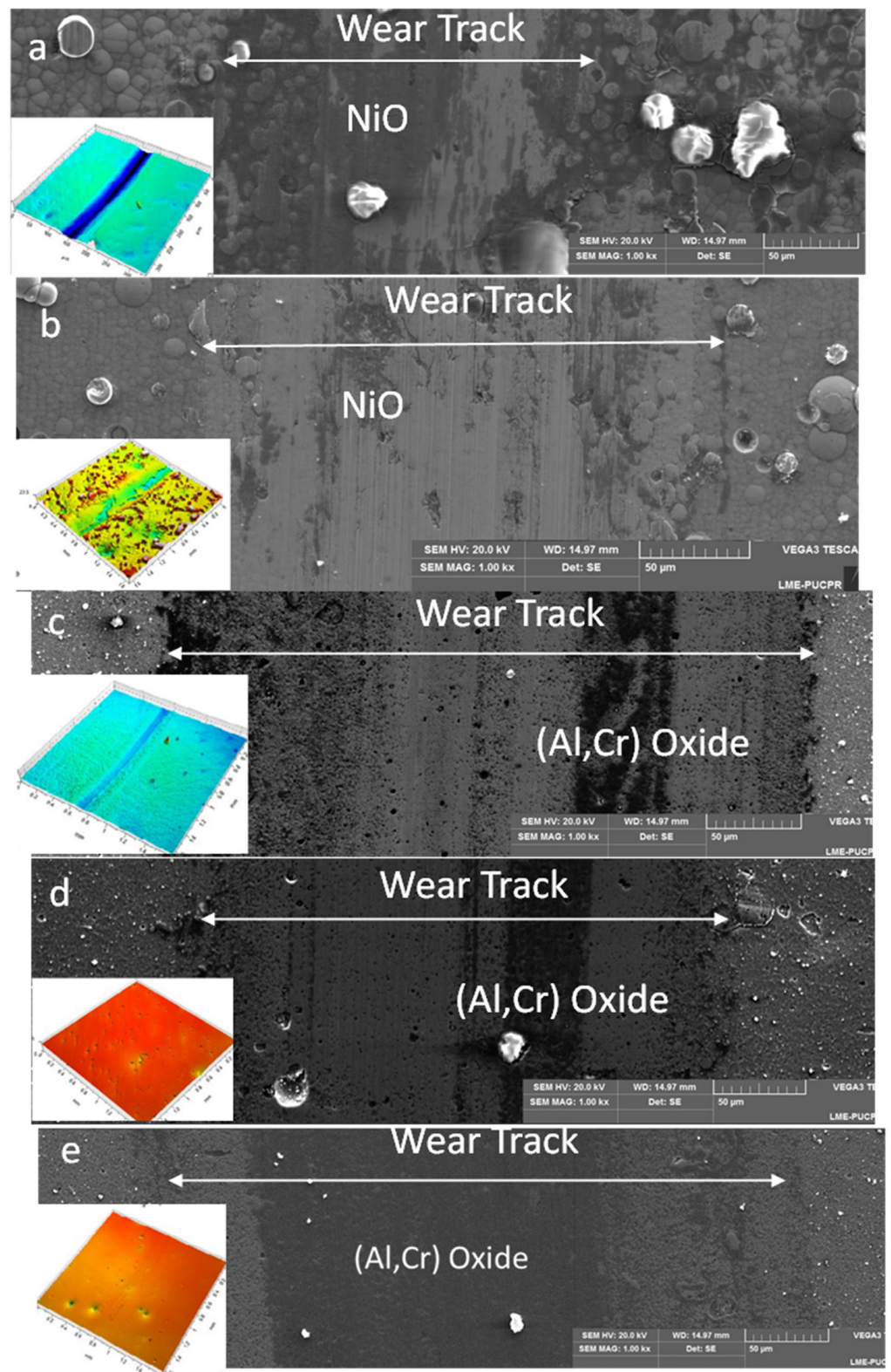


Figure 6. Aspect of the wear tracks: (a) NiP IPHT at 400 °C/nitrided steel; (b) NiP IPHT at 610 °C/nitrided steel; (c) AlCrN/nitrided steel; (d) AlCrN/NiP IPHT at 400 °C/nitrided steel; and (e) AlCrN/NiP IPHT at 610 °C/nitrided steel architectures.

For the NiP IPHT at 400 °C, the coefficient of friction behavior reveals a plateau at 0.34, associated with the removal of the cauliflower layer. The outer cauliflower layer exhibits poor adhesion to the NiP deposit, easily sheared from the specimen surface. Following this

initial phase, an increase in the coefficient of friction is observed, likely attributed to the work hardening of the NiP deposit and the formation of NiO (according to EDS results) due to the sliding contact, as depicted in Figure 6a. The wear rate (Figure 7) is not constant; it increases with sliding distance, reaching its maximum value at 500 m, coinciding with the removal of the cauliflower layer. Subsequently, the formation of NiO and the work hardening contribute to a decrease in the wear rate, observed at 1000 m of sliding.

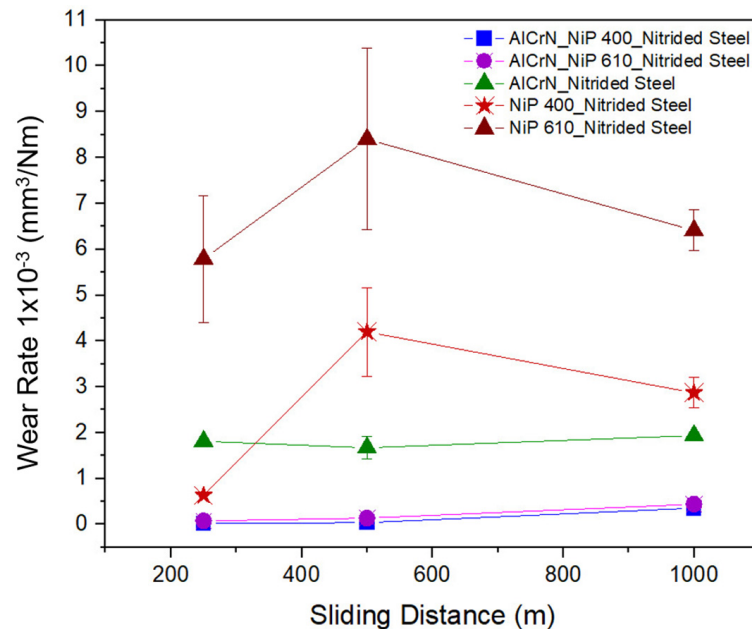


Figure 7. Wear rate with the sliding distance of the five architectures.

On the contrary, when the NiP deposit undergoes interdiffusion post-heat treatment (IPHT) at 610 °C, a shift in the friction coefficient behavior is observed compared to NiP IPHT at 400 °C (Figure 5). The friction coefficient exhibits an unstable pattern, potentially attributed to the presence of the NiO layer (according to EDS results) formed due to exposure to the elevated temperature of 610 °C and the concurrent removal and redeposition of NiP. The reported thickness of the NiO layer formed during the interdiffusion heat treatment ranges between 0.5 and 1 μm [13]. Plow lines, indicative of a two-body wear mechanism, are observed in Figure 6b. The wear rate in Figure 7 follows a similar trend observed for NiP IPHT at 400 °C.

Comparing the friction coefficient of AlCrN over NiP IPHT at 400 °C in Figure 5 with AlCrN directly over the nitrided substrate in Figure 6a reveals that AlCrN over NiP IPHT at 400 °C exhibits a lower friction coefficient. The steady-state coefficient of friction (COF) is 0.47 when AlCrN is over NiP IPHT at 400 °C, while the COF is 0.53 when AlCrN is over a nitrided steel substrate. Another distinction between the two substrates is the absence of an increase in COF during the initial sliding meters when AlCrN is over NiP substrates.

A clear difference in the friction coefficient is evident between AlCrN over NiP IPHT at 400 °C and 610 °C (Figure 5). Moreover, the steady-state friction coefficient for AlCrN over NiP IPHT at 610 °C is approximately 0.6 higher than AlCrN over NiP at 400 °C (i.e., 0.47). The primary wear mechanism is oxidative because chromium, aluminum, and oxygen signals overlap, according to EDS, consistent with the behavior observed when AlCrN is over nitrided steel, as indicated in Figure 6d,e, respectively. The wear rate for AlCrN over NiP IPHT at 400 °C or 610 °C (Figure 7) is practically identical, and the wear rate remains constant throughout the sliding distance.

The H/E ratio, a widely used predictor of wear performance, is presented in Table 2 for all five architectures, along with the H/E for the nitrided case [36]. One can realize a sound correlation between the wear rate of the duplex architectures and their H/E ratio. For instance, the H/E ratios of the NiP IPHT at 400 °C, NiP IPHT at 610 °C, and AlCrN

over nitrided are 0.064, 0.053, and 0.1, respectively. Examining the wear rates (Figure 7), it becomes evident that the AlCrN over the nitrided substrate exhibits the lowest wear rate, while the wear rate is highest for the NiP IPHT at 610 °C. On the other hand, the triplex architecture shows an H/E ratio of around 0.09, regardless of the NiP microstructure, and, interestingly, the wear rates for both architectures are comparable.

4. Conclusions

The tribological behavior of duplex and triplex architectures was meticulously investigated. The duplex configuration, whether it was AlCrN or NiP coatings on a nitrided steel substrate, and the triplex architecture, where AlCrN was deposited on the NiP-coated surface in the previously nitrided steel substrate, were thoroughly examined. In both duplex and triplex architectures, the NiP underwent interdiffusion post-heat treatment at either 400 °C or 610 °C. The following conclusions can be drawn:

The interdiffusion post-heat treatment (IPHT) played a pivotal role in the mechanical behavior of the duplex and triplex architectures, particularly in the NiP deposits. The microstructure resulting from the IPHT at 400 °C comprised Ni and coherent Ni₃P, while the IPHT at 610 °C led to a microstructure consisting of Ni, NiO, and incoherent Ni₃P. This significant difference in microstructure resulted in higher H and E for the NiP IPHT at 400 °C. Comparatively, AlCrN over a nitrided substrate showed H and E higher than AlCrN over the NiP deposit.

One of the key findings of this research was the poor adhesion of the AlCrN over the NiP deposit, a significant observation, regardless of the IPHT temperature. The adhesion of AlCrN on the NiP deposit showed gross spallation, indicating poor adhesion.

The coefficient of friction of the AlCrN over a nitrided steel surface showed an initial increase during the early stages of sliding. This was attributed to the presence of droplets on the coated surface, which act as frictional hotspots. Once these droplets were removed, the COF decreased and reached a steady state, stabilizing at approximately 0.53. The lowest COF was observed when AlCrN was over NiP IPHT at 400 °C, indicating the superior tribological performance of this architecture. The wear mechanism remained oxidative, regardless of the NiP IPHT temperature. The wear rate of AlCrN over NiP IPHT at 400 °C was the lowest, while NiP over the nitrided steel substrate exhibited the highest wear rate. The formation of NiO due to sliding contact contributed to increased wear resistance in the NiP deposit. Notably, a strong correlation was observed between the H/E ratio and the wear rates in both the duplex and triplex architectures, highlighting the importance of this ratio in predicting the wear behavior of the coatings.

Author Contributions: Conceptualization, M.E.S.; Methodology, Q.H. and B.M.d.F.; Formal analysis, B.M.d.F. and P.S.; Resources, F.L.A.; Data curation, F.L.A.; Writing—original draft, P.S.; Writing—review & editing, J.M.D. and S.C.V.; Supervision, R.D.T. All authors have read and agreed to the published version of the manuscript.

Funding: This research received no external funding. The APC was funded by McMaster and MDPI.

Data Availability Statement: Data are contained within the article.

Conflicts of Interest: The authors declare no conflict of interest.

References

1. Henriques, C.C.D.; Joia, C.-J.B.; Guedes, F.; Baptista, I.P. Material Selection for Brazilian Presalt Fields. In Proceedings of the Offshore Technology Conference, Houston, Texas, USA, 30 April–3 May 2012; p. OTC-23320-MS. [\[CrossRef\]](#)
2. Iannuzzi, M.; Barnoush, A.; Johnsen, R. Materials and corrosion trends in offshore and subsea oil and gas production. *Npj Mater. Degrad.* **2017**, *1*, 2. [\[CrossRef\]](#)
3. Sudagar, J.; Lian, J.; Sha, W. Electroless nickel, alloy, composite and nano coatings—A critical review. *J. Alloys Compd.* **2013**, *571*, 183–204. [\[CrossRef\]](#)
4. Mallory, G. The Fundamental Aspects of Electroless Nickel Plating. *Electroless Plat. Fundam. Appl.* **1991**, 1–56.
5. Fayyad, E.M.; Abdullah, A.M.; Hassan, M.K.; Mohamed, A.M.; Jarjoura, G.; Farhat, Z. Recent advances in electroless-plated Ni-P and its composites for erosion and corrosion applications: A review. *Emergent Mater.* **2018**, *1*, 3–24. [\[CrossRef\]](#)

6. Rabizadeh, T.; Allahkaram, S.R.; Zarebidaki, A. An investigation on effects of heat treatment on corrosion properties of Ni-P electroless nano-coatings. *Mater. Des.* **2010**, *31*, 3174–3179. [[CrossRef](#)]
7. Taheri, R.; Oguocha, I.N.A.; Yannacopoulos, S. The tribological characteristics of electroless NiP coatings. *Wear* **2001**, *249*, 389–396. [[CrossRef](#)]
8. Keong, K.G.; Sha, W.; Malinov, S. Hardness evolution of electroless nickel-phosphorus deposits with thermal processing. *Surf. Coatings Technol.* **2003**, *168*, 263–274. [[CrossRef](#)]
9. Keong, K.G.; Sha, W. Crystallisation and Phase Transformation Behaviour of Electroless Nickel-Phosphorus Deposits and Their Engineering Properties. *Surf. Eng.* **2002**, *18*, 329–343. [[CrossRef](#)]
10. Ramalho, A.; Miranda, J.C. Friction and wear of electroless NiP and NiP + PTFE coatings. *Wear* **2005**, *259*, 828–834. [[CrossRef](#)]
11. Zangeneh-Madar, K.; Vaghefi, S.M.M. The effect of thermochemical treatment on the structure and hardness of electroless Ni-P coated low alloy steel. *Surf. Coatings Technol.* **2004**, *182*, 65–74. [[CrossRef](#)]
12. Soares, M.E.; Soares, P.; Souza, P.R.; Souza, R.M.; Torres, R.D. The effect of nitriding on adhesion and mechanical properties of electroless Ni-P coating on AISI 4140 steel. *Surf. Eng.* **2016**, *33*, 1–6. [[CrossRef](#)]
13. Correia, K.S.; Greca, L.G.; Sopchenski, L.; Soares, P.; Amorim, F.L.; Torres, R.D. Strength and Deformation Properties of Low-Alloy Steel Bolts with Electroless Ni-P Coating: An Investigation of Two Thermal Routes. *J. Mater. Eng. Perform.* **2020**, *29*, 6025–6032. [[CrossRef](#)]
14. Hsu, C.; Chiu, S.; Shih, Y. Effects of thickness of electroless Ni-P deposit on corrosion fatigue damage of 7075-T6 under salt spray atmosphere. *Mater. Trans.* **2004**, *45*, 3201–3208. [[CrossRef](#)]
15. Hsu, C.H.; Lee, C.Y.; Chen, K.L.; Lu, J.H. Effects of CrN/EN and Cr₂O₃/EN duplex coatings on corrosion resistance of ADI. *Thin Solid Films* **2009**, *517*, 5248–5252. [[CrossRef](#)]
16. Hudak, O.E.; Kutrowatz, P.; Wojcik, T.; Ntemou, E.; Primetzhofer, D.; Shang, L.; Ramm, J.; Hunold, O.; Kolozsv, S.; Polcik, P.; et al. Improved corrosion resistance of cathodic arc evaporated Al_{0.7}Cr_{0.3-x}V_xN coatings in NaCl-rich media. *Corros. Sci.* **2023**, *221*, 11376. [[CrossRef](#)]
17. Li, Y.Y.; Wu, F.B. Microstructure and corrosion characteristics of CrN/NiP sputtering thin films. *Thin Solid Films* **2010**, *518*, 7527–7531. [[CrossRef](#)]
18. Biswas, B.; Purandara, Y.; Khan, I.; Hovsepian, P.E. Effect of substrate bias voltage on defect generation and their influence on corrosion and tribological properties of HIPIMS deposited CrN/NbN coatings. *Surf. Coatings Technol.* **2018**, *344*, 383–393. [[CrossRef](#)]
19. Sánchez, J.E.; Sánchez, O.M.; Ipaz, L.; Aperador, W.; Caicedo, J.C.; Amaya, C.; Landaverde, M.A.H.; Beltran, F.E.; Muñoz-Saldaña, J.; Zambrano, G. Mechanical, tribological, and electrochemical behavior of Cr_{1-x}Al_xN coatings deposited by r.f. reactive magnetron co-sputtering method. *Appl. Surf. Sci.* **2010**, *256*, 2380–2387. [[CrossRef](#)]
20. Petrogalli, C.; Montesano, L.; Gelfi, M.; La Vecchia, G.M.; Solazzi, L. Tribological and corrosion behavior of CrN coatings: Roles of substrate and deposition defects. *Surf. Coatings Technol.* **2014**, *258*, 878–885. [[CrossRef](#)]
21. Panjan, P.; Čekada, M.; Panjan, M.; Kek-Merl, D.; Zupanič, F.; Čurković, L.; Paskvale, S. The Surface density of growth defects in different PVD hard coatings prepared by sputtering. *Vacuum* **2012**, *86*, 794–798. [[CrossRef](#)]
22. Mo, J.L.; Zhu, M.H.; Leyland, A.; Matthews, A. Impact wear and abrasion resistance of CrN, AlCrN and AlTiN PVD coatings. *Surf. Coatings Technol.* **2013**, *215*, 170–177. [[CrossRef](#)]
23. Liew, W.Y.H.; Jie, J.L.L.; Yan, L.Y.; Dayou, J.; Sipaut, C.S.; Madlan, M.F.B. Frictional and wear behaviour of AlCrN, TiN, TiAlN single-layer coatings, and TiAlN/AlCrN, AlN/TiN nano-multilayer coatings in dry sliding. *Procedia Eng.* **2013**, *68*, 512–517. [[CrossRef](#)]
24. Ballesteros-Arguello, A.; Ramírez-Reyna, F.O.; Rodríguez-Castro, G.A.; Meneses-Amador, A.; Fernández-Valdés, D.; Reyes-Carcaño, O. Experimental and numerical evaluation of the contact fatigue resistance of AlCrN, Fe_xN and AlCrN/Fe_xN coatings on AISI 4140 steel. *Surf. Coatings Technol.* **2021**, *423*, 127620. [[CrossRef](#)]
25. Mo, J.L.; Zhu, M.H.; Lei, B.; Leng, Y.X.; Huang, N. Comparison of tribological behaviours of AlCrN and TiAlN coatings-Deposited by physical vapor deposition. *Wear* **2007**, *263*, 1423–1429. [[CrossRef](#)]
26. ASTM C 1624-22; Standard Test Method for Adhesion Strength and Mechanical Failure Modes of Ceramic Coatings by Quantitative Single Point Scratch Testing. ASTM International: West Conshohocken, PA, USA, 2022. [[CrossRef](#)]
27. ASTM G99-17; Standard Test Method for Wear Testing with a Pin-on-Disk Apparatus. ASTM International: West Conshohocken, PA, USA, 2020. [[CrossRef](#)]
28. Islam, M.; Azhar, M.R.; Fredj, N.; Burleigh, T.D. Electrochemical impedance spectroscopy and indentation studies of pure and composite electroless Ni-P coatings. *Surf. Coatings Technol.* **2013**, *236*, 262–268. [[CrossRef](#)]
29. Sahoo, P.; Das, S.K. Tribology of electroless nickel coatings—A review. *Mater. Des.* **2011**, *32*, 1760–1775. [[CrossRef](#)]
30. Rajendran, R.; Sha, W.; Elansezhian, R. Abrasive wear resistance of electroless Ni-P coated aluminium after post treatment. *Surf. Coatings Technol.* **2010**, *205*, 766–772. [[CrossRef](#)]
31. Chen, J.-S.; Yu, C.; Lu, H. Phase stability, magnetism, elastic properties and hardness of binary iron nitrides from first principles. *J. Alloys Compd.* **2015**, *625*, 224–230. [[CrossRef](#)]
32. Apachitei, I.; Tichelaar, F.D.; Duszczuk, J.; Katgerman, L. The effect of heat treatment on the structure and abrasive wear resistance of autocatalytic NiP and NiP-SiC coatings. *Surf. Coatings Technol.* **2002**, *149*, 263–278. [[CrossRef](#)]

33. Malfatti, C.F.; Veit, H.M.; Santos, C.B.; Metzner, M.; Hololeczek, H.; Bonino, J.P. Heat treated NiP-SiC composite coatings: Elaboration and tribocorrosion behaviour in NaCl solution. *Tribol. Lett.* **2009**, *36*, 165–173. [[CrossRef](#)]
34. Reiter, A.E.; Derflinger, V.H.; Hanselmann, B.; Bachmann, T.; Sartory, B. Investigation of the properties of Al_{1-x}Cr_xN coatings prepared by cathodic arc evaporation. *Surf. Coatings Technol.* **2005**, *200*, 2114–2122. [[CrossRef](#)]
35. Ramírez-Reyna, F.O.; Rodríguez-Castro, G.A.; Figueroa-López, U.; Morón, R.C.; Arzate-Vázquez, I.; Meneses-Amador, A. Effect of nitriding pretreatment on adhesion and tribological properties of AlCrN coating. *Mater. Lett.* **2021**, *284*, 128931. [[CrossRef](#)]
36. Kumar, A.; Li, D.Y. Can the H/E ratio be generalized as an index for the wear resistance of materials? *Mater. Chem. Phys.* **2022**, *275*, 125245. [[CrossRef](#)]

Disclaimer/Publisher’s Note: The statements, opinions and data contained in all publications are solely those of the individual author(s) and contributor(s) and not of MDPI and/or the editor(s). MDPI and/or the editor(s) disclaim responsibility for any injury to people or property resulting from any ideas, methods, instructions or products referred to in the content.